DOI 10.1007/s10812-024-01817-6
Journal of Applied Spectroscopy, Vol. 91, No. 5, November, 2024 (Russian Original Vol. 91, No. 5, September–October, 2024)

QUANTUM CHEMICAL CALCULATION OF THE FIELD ELECTRON EMISSION THRESHOLD FROM SHORT BORON-NITRIDE NANOTUBES

O. B. Tomilin,[a] E. V. Rodionova,[a,*] E. A. Rodin,[a] N. A. Poklonski,[b,*] and A. V. Knyazev[c]

UDC 544.032,544.169

The electronic structure of cylindrical conjugated macromolecules of boron and nitrogen atoms modeling short open nanotubes of zigzag (n,0) and armchair types (n,n) was calculated using density functional theory with the B3LYP hybrid functional in the 6–31G basis set. Their stability as a function of diameter and length was studied. It was shown that a constant electric field applied along the tubes led to a compression of the energy gap in the electron energy spectrum of the nanotubes up to ≈0.2 eV. The threshold of field electron emission from boron-nitride nanotubes was calculated in the framework of the emission molecular orbitals theory. It was shown that, despite conjugated systems of boron-nitride and carbon nanotubes being isoelectronic, substitution of carbon atoms in the nanotube framework of nitrogen and boron atoms led to a decrease in the threshold field strength of the field emission. It was found that the diameter of boron-nitride nanotubes had virtually no effect on the emission molecular orbital.

Keywords: *conjugated boron-nitride cylindrical macromolecules, boron-nitride nanotubes, field electron emission, energy gap.*

Introduction. Carbon nanotubes (CNTs) are promising materials for cathode of vacuum microelectronics [1, 2], flat displays [3, 4], sensor devices [5, 6], and lighting elements [7, 8]. The theory of fi eld electron emission from CNTs has a unique history. Initially, the Fowler–Nordheim (FN) theory of fi eld electron emission, which was developed for metal cathodes [9], was used to interpret the experimental data. The FN theory represents emission of electrons from a cathode (emitter) into a vacuum as a tunneling transition of them through a potential barrier with consideration of the Coulomb potential of the emitted electron image in the cathode. The electron work function of the emitter was considered constant over the whole range of applied electric fi eld strength [10]. The FN theory also did not consider the geometric structure of the cathode surface [11]. A key result of the FN theory was the prediction of a linear dependence of $\ln (J/F^2)$ on $1/F$, where J is the electron emission current density and F, the external stationary uniform electric field strength.

Experimental data for field electron emission from CNTs showed that the dependence of $\ln (J/F^2)$ on $1/F$ was nonlinear [12–14]. Considering this, introduction of correction factors into the FN formula was proposed without discussing their physical meaning [15]. Also, the calculated and experimental values of the work function from CNTs were observed to differ [16]. Furthermore, the dependence of the emission current density J on electric field strength F could be represented as two intersecting lines with positive slopes θ [12, 17–19]. For small values of F, angle $\theta \to 0$ although $\theta \to \pi/2$ starting from a certain threshold value F_{cr}. This dependence of J on F indicated that the external electric field F had a significant influence on the work function of an electron into a vacuum [10]. The experimentally recorded photoluminescence for field emission from CNTs also was not theoretically supported [17].

Two reasons were responsible for the above unsolved problems with a theoretical description of field electron emission from CNTs. 1) CNTs are quasi-one-dimensional systems for which the concept of a potential image is inapplicable. The problem of a correct description of the potential barrier for an electron tunneling transition is not yet finally solved. Therefore, the justification for the assumption made in FN theory about the work function of an electron from a cathode being independent of the external electric field strength is dubious [10]. 2) The geometric structure and electronic structure

*To whom correspondence should be addressed.

[a]Mordovia State University, Saransk, Russia; email: Rodionova_j87@mail.ru; [b]Belarusian State University, Minsk, Belarus; email: Poklonski@bsu.by; [c]Lobachevsky State University, Nizhny Novgorod, Russia. Translated from Zhurnal Prikladnoi Spektroskopii, Vol. 91, No. 5, pp. 699-708, September–October, 2024. Original article submitted July 5, 2024.

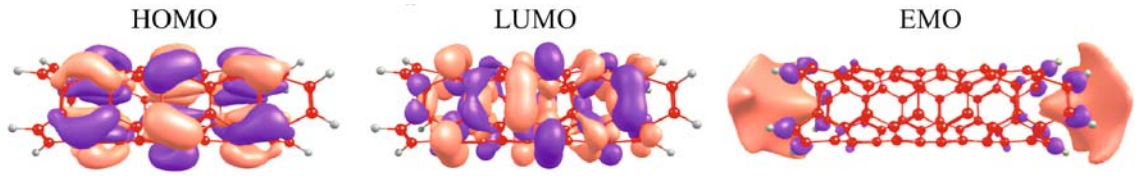

Fig. 1. Diagram (from the literature [28]) of electron density distribution in highest occupied (HOMO), lowest unoccupied (LUMO), and emission molecular orbitals (EMO) in three short open CNT of type (3,3) of the same length without an external electric field; C atoms on ends of nanotubes were passivated with H atoms.

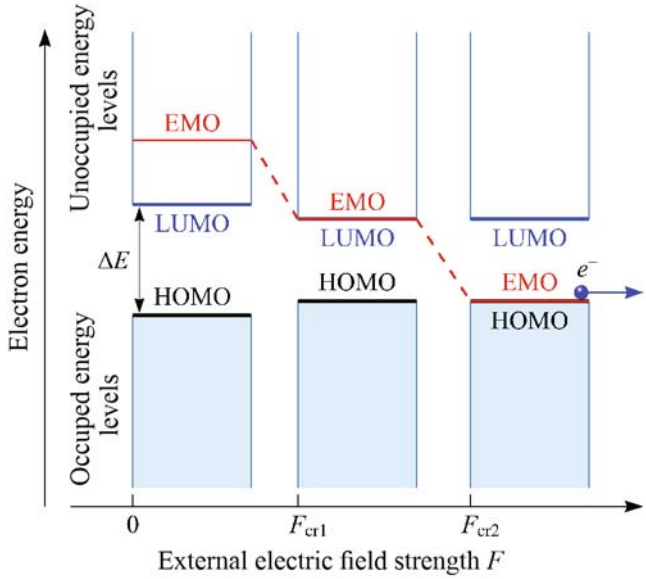

Fig. 2. Diagram of change of energy diagram of CNT (ΔE is the energy gap) upon increasing the field strength along the tube followed by field emission of electrons (e^-) into a vacuum.

of the ends (caps [20]) of CNTs play a decisive role in field emission in them. Pentagons existing in the CNT cap generate localized electronic states [molecular orbitals (MOs)], i.e., emission molecular orbitals (EMOs), that provide a high current density of emission electrons [21, 22]. Hence, the current stage of describing field electron emission from CNTs is related to the need to consider the electronic structure of CNTs and the features of its change in an external electrical field.

Postulation of the existence in open and closed CNTs of unoccupied electronic states localized on the ends of spatial elements (end areas) of CNTs that were generated by defects decorating the CNT apex was the starting point for a theory of field emission different from FN theory [23, 24]. It was shown in terms of an *ab initio* method [25] that such unoccupied MOs shifted into the CNT valence band under the action of an applied constant electric field. Charge redistributed during this transition through the carbon framework of the nanotube. This led to the accumulation of electrons on its apex. This was responsible for the physical prerequisites for reducing the effective work function [26]. According to the literature [25], the region of localization of electrons in an EMO on the CNT ends is 0.4–0.5 nm. The emission current from the localized electronic states is an order of magnitude greater than the contribution from states of higher occupied molecular orbitals (HOMOs) of the valence band.

The mechanism of field electron emission from CNTs was further developed [27]. The threshold external electric field strength F_{cr} was estimated. This mechanism included accumulation of electrons on the apical regions of nanotubes [28] followed by their tunneling into a vacuum. Calculations showed [29] that in-plane electronic conjugation [30] leading to the appearance of MOs ensuring localization of electrons in the CNT apical regions existed in the conjugated system of

CNT π-electrons. These EMOs were degenerate and unoccupied (free) for electrons (Fig. 1). The EMO energy was highly sensitive to external electric field strength *F*. Some of the formed EMOs shifted into the CNT valence band as *F* increased. The EMOs were filled with electrons by accumulation of electrons in the CNT apical regions followed by their tunneling into a vacuum (Fig. 2).

The appearance of unoccupied MOs in the CNT valence band qualitatively explained the experimentally observed luminescence from CNT apexes that was induced by a constant electric field [17, 31, 32]. Thus, the analysis of the behavior of EMO energy in a constant electric field could link the CNT electronic structure to their emission properties and estimate the threshold strength F_{cr} for appearance of an emission current.

The mechanism of field electron emission from CNTs presented above opened possibilities for controlling their parameters upon CNT modification. Partial or complete substitution of C-atoms in the framework by heteroatoms is one direction for modification of carbon nanostructures with conjugated systems of π-electrons. For example, CNT doped with N, B, Ge, and Al atoms have been prepared experimentally [33]. Stoichiometric boron-nitride nanotubes (BN-nanotubes) isoelectronic to CNTs have also been prepared [34].

Boron-nitride nanotubes (BNNTs) are mechanically strong (like CNTs) and have high thermal conductivity, resistance to oxidation, negative affinity for an electron, and high thermal stability as compared to CNTs [35]. They have been used independently as a cathode material and an additive component for improving the properties of a composite [36].

The aim of the present work was to study the electronic properties of BNNTs of various diameters, lengths, and chirality and their emission properties based on the fi eld electron emission theory from CNTs [27, 28].

Research Model and Methodology. Model short single-walled cylindrical BNNTs of chirality (*n*,0) and (*n*,*n*) were selected for the study. Model nanotubes with various diameters and lengths were studied to evaluate the influence of the geometric parameters of BNNTs on their electronic and emission properties. The diameter was determined by chirality indices $n = 5, 7$ for *zigzag* nanotubes (*n*,0) and $n = 3, 4$ for *armchair* nanotubes (*n*,*n*). The linear length of the model BNNTs was determined by the number of interacting cyclic *trans*- and *cis*-BN atomic chains situated in the cross section perpendicular to the axial symmetry axis of the hollow cylindrical nanotubes. The length of the examined nanotubes varied from 2 to 10 cyclic BN atomic chains. The free valences of terminal atoms in the examined model molecular systems were saturated by H atoms. Thus, the number of all atoms in the model macromolecules varied from 30 (for $B_{10}N_{10}H_{10}$) to 176 (for $B_{80}N_{80}H_{16}$).

The geometry was optimized and the energy characteristics of the model molecules were calculated using density functional theory (DFT) with hybrid functional B3LYP in basis set 6-31G from the FireFly applied program suite [37]. Self-consistent procedures found extreme points on the potential energy surface obtained from eigenvalues of the Hess operator.

The effect of an external uniform stationary electric field on the electronic and emission properties of BNNTs was numerically modeled using EFIELD options of the FireFly applied program suite. Electric field force lines were directed along the axial axis of each nanotube. Because terminal chains in nanotubes of chirality (*n*,0) were nonequivalent, two possible directions of the applied vector of the electric field strength were examined (Fig. 3). The strength of the constant electric field *F* was varied in the range 0–30 V/nm in steps of 1 V/nm.

Results and Discussion. *Stability of model BNNTs.* The relative stability of BNNTs was estimated by calculating the atomization energy E_{at} attributed to each atom using the formula:

$$E_{at} = \frac{x(E_N + E_B) + yE_H - E_{B_xN_xH_y}}{2x + y}, \quad (1)$$

where E_N is the energy of an N atom; E_B, the energy of a B atom; E_H, the energy of an H atom; $2x$, the total number of N and B atoms; y, the number of H atoms on nanotube apices; and $E_{B_xN_xH_y}$, the energy of the model BNNTs.

Table 1 presents the E_{at} values obtained using Eq. (1). The E_{at} values found for all examined BNNTs were positive, i.e., existence of cylindrical macromolecules was energetically more favorable than the same number (as in the tube) of separate B and N atoms. The relative stability of the BNNTs increased with increasing diameter and length. This was due to an increase in the number of B and N atoms in the BNNTs increasing the number of π-electrons in the conjugated system, thereby increasing the stabilizing action of electrons in the BNNT framework with ionic-covalent chemical bonds.

Electronic properties of model BNNTs. Let us examine the electronic properties of the studied BN nanotubes using as an example the change of the energy gap ΔE, which is the difference between the lowest unoccupied (LUMO) and highest occupied electronic molecular orbitals (HOMO) distributing electron density throughout the nanotube framework:

$$\Delta E = E_{LUMO} - E_{HOMO}. \quad (2)$$

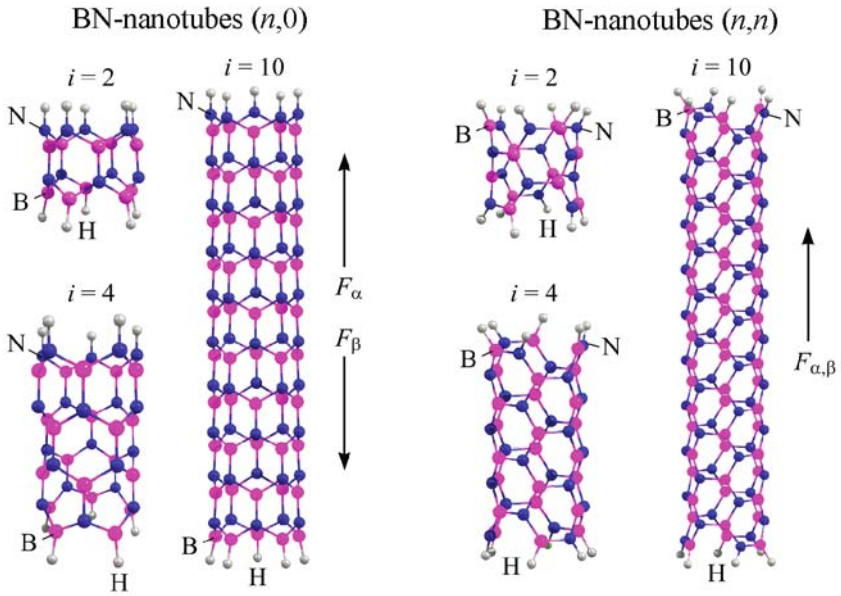

Fig. 3. Diagram of three BN nanotubes of type (*n*,0) and three of type (*n*,*n*) as systems of interacting cyclic (circular) *trans*- and *cis*-atomic chains (*i*, number of rings) and direction of strength vector *F* (with indices α and β) of external stationary uniform electric field along nanotubes.

TABLE 1. Atomization Energy E_{at} (eV) of Boron-Nitride Nanotubes of Various Lengths

Nanotube length	Chirality index			
	(5,0)	(7,0)	(3,3)	(4,4)
i = 2	5.72	5.85	5.81	5.89
i = 4	6.45	6.61	6.52	6.63
i = 6	6.76	6.94	6.82	6.95
i = 10	7.05	7.23	7.10	7.22

Table 2 presents the Δ*E* values calculated using Eq. (2) for CNTs and BNNTs with a linear length of *i* = 6 interacting C and BN cyclic chains. The Δ*E* values for BNNTs were observed to increase smoothly upon increasing their diameter and exceeded Δ*E* for pure CNTs [38]. Similar results were obtained before [39, 40]. The Δ*E* value asymptotically approached the width of the energy bandgap (≈6 eV) of planar hexagonal BN upon increasing the BNNT diameter [41].

According to experimental data, BNNTs are broadband semiconductors [42, 43]. The bandgap width of BNNTs according to various estimates varies from 5.4 to 6 eV. Thus, the calculated values (Table 2) agreed with the experimental data.

An increase in the linear length as a function of the BNNT chirality had a different effect on the energy gap Δ*E* (Table 3). For example, the Δ*E* value for BNNTs of type (*n*,0) decreased asymptotically with increasing length of the nanostructure. However, the Δ*E* value was practically independent of nanotube length for BNNTs of type (*n*,*n*).

Figure 4 shows dependences of Δ*E* on electric field strength *F* for BNNTs of various lengths. The energy gap Δ*E* was visibly compressed regardless of the length of the BNNT and the direction of electric field strength vector *F*. Note that the decrease of Δ*E* to a certain relative constant value was rather large. This trend stabilized with the length of the examined BNNTs having the number of rings *i* ≥ 6. For example, the Δ*E* value with *i* = 6 (Fig. 3) for BNNTs reached 0.2 eV starting with electric field strength *F* ≈ 9 V/nm and was about the same upon increasing the field strength further.

TABLE 2. Energy Gap ΔE (eV) of Single-Walled Carbon Nanotubes (CNT) and Boron-Nitride Nanotubes (BNNT) of Various Chirality (for $i = 6$)

Nanotube type	Chirality index			
	(5,0)	(7,0)	(3,3)	(4,4)
CNT	1.59	2.59	1.84	1.18
BNNT	3.41	4.90	6.00	6.03

TABLE 3. Energy Gap ΔE (eV) of Boron-Nitride Nanotubes of Various Lengths (Fig. 3)

BN-nanotube length	Chirality index			
	(5,0)	(7,0)	(3,3)	(4,4)
$i = 2$	4.49	5.85	6.12	6.22
$i = 4$	3.80	5.22	5.99	6.06
$i = 6$	3.41	4.90	6.00	6.03
$i = 10$	2.98	4.58	6.00	6.00

Note that compression of the energy gap under the influence of an applied constant electric field was also observed in CNTs. The calculations showed that $\Delta E = 0.4$–0.5 eV for CNTs after compression at $F \approx 9$ V/nm. This was about double the value for BNNTs. This difference was due to BNNTs being systems of interacting electric dipoles (B–N chemical bonds), in contrast to CNTs.

The results agreed with experimental and calculated data obtained in several investigations. For example, a substantial decrease in the energy bandgap width ΔE of BNNTs in an external constant electric field was reported [44, 45]. A non-monotonic change of the energy gap of CNTs could also occur upon their mechanical deformation [46].

Emission properties of model BNNTs. Calculations of the electronic structure of model BNNTs showed that EMOs existed on the end planes of all examined nanotubes. These orbitals were characterized by preferential localization of electron density on the apices of nanotubes even without an external electric field (Fig. 1 for CNTs). The EMOs in the energy spectrum were gathered into groups differing in the number of nodes L of sign inversion of wave functions in the EMO basis expansion.

The first group (I) of EMOs was represented by two unoccupied MOs for $L = 2$. These EMOs for CNTs were degenerate with respect to energy. The degeneracy of EMOs (I) was lifted for BNNTs because of the difference in the electronegativities of the atoms.

The second group (II) of EMOs consisted of four unoccupied MOs with similar energies for $L = 4$. The EMO energy increased with increasing number of nodes L of atomic wave functions. Therefore, EMOs of the third group (III) for $L = 8$ lay deep within the conductivity band. These features of the EMOs were observed in the energy spectra of all examined BNNTs.

The discussion of the emission properties of BNNTs was limited to a description of trends in the change of EMO energy for $L = 2$ in a constant external electric field. Let us examine the behavior of the energy of boundary (HOMO and LUMO) and emission (EMO) molecular orbitals of model BNNTs in an external uniform stationary electric field.

Let the field strength vector be directed along the nanotube axial axis (Fig. 3). The energies of boundary MOs, i.e., HOMO (E_{HOMO}) and LUMO (E_{LUMO}), vary in an external electric field in approaching directions; the energies of the EMOs (E_{EMO1}, E_{EMO2}), in the opposite directions. Energy gap ΔE is compressed to a certain value ($\approx$0.2 eV) for field strength $F > 9$ V/nm. This persists upon increasing F further. The energy of one of the EMOs (E_{EMO1}) decreases in the electric field. The EMO energy reaches the LUMO energy for field strength $F = F_{\mathrm{cr1}}$ and then the HOMO energy for $F = F_{\mathrm{cr2}}$. The EMO transition into the valence band is accompanied by filling of the emission state with electrons. This ensures physical conditions for field electron emission from the nanotube via tunneling into the vacuum. The energy of the

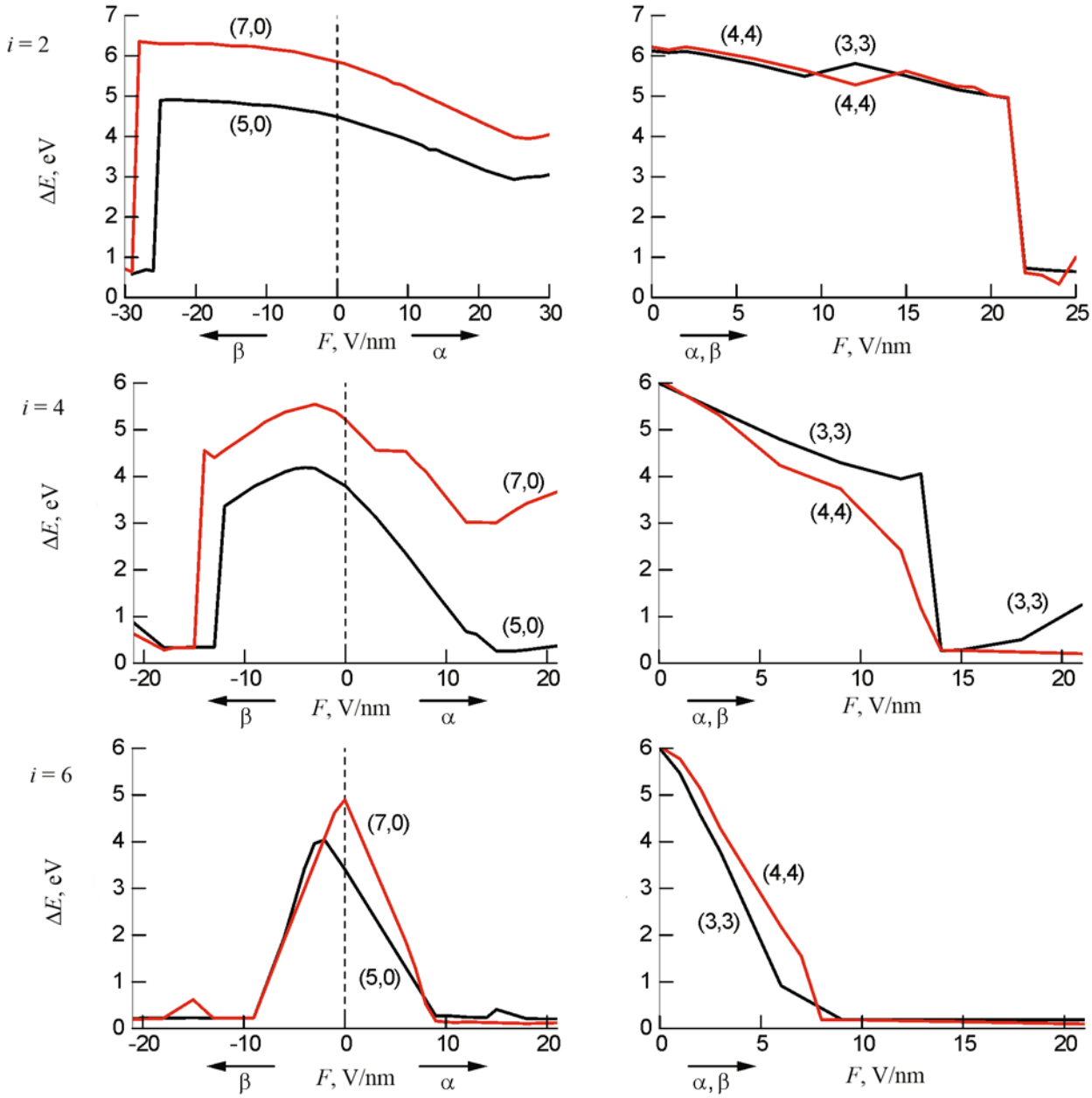

Fig. 4. Dependences of energy gap ΔE on external uniform stationary electric field strength along BN-nanotubes (i = 2, 4, 6).

other EMO (E_{EMO2}) increases significantly upon increasing the electric field strength and is uninteresting for describing emission spectra of the nanotubes.

Figures 5 and 6 show dependences of energy E of boundary and emission MOs on the strength of the applied constant electric field for single-walled BNNTs. Figures 5 and 6 and Table 4 show that the EMO energy reaches the LUMO energy for $|F_{cr1}| \le 12$ V/nm, i.e., in the region after compression of the energy gap under the influence of a constant electric field for (n,0). The EMO energy transitioned into the region of valence band energies for $|F_{cr2}| \le 13$ V/nm.

Let us compare critical strengths F_{cr1} and F_{cr2} of model CNTs and BNNTs. Table 4 shows that the emission properties of the studied BN nanotubes exceeded those of CNTs [47]. This was due to the larger compression of the energy gap in BNNTs, which led to a decrease in the threshold strength of the external field electron emission, as noted before [48]. The field strength required to fill the EMOs with electrons for BNNTs was practically independent of the nanotube diameter

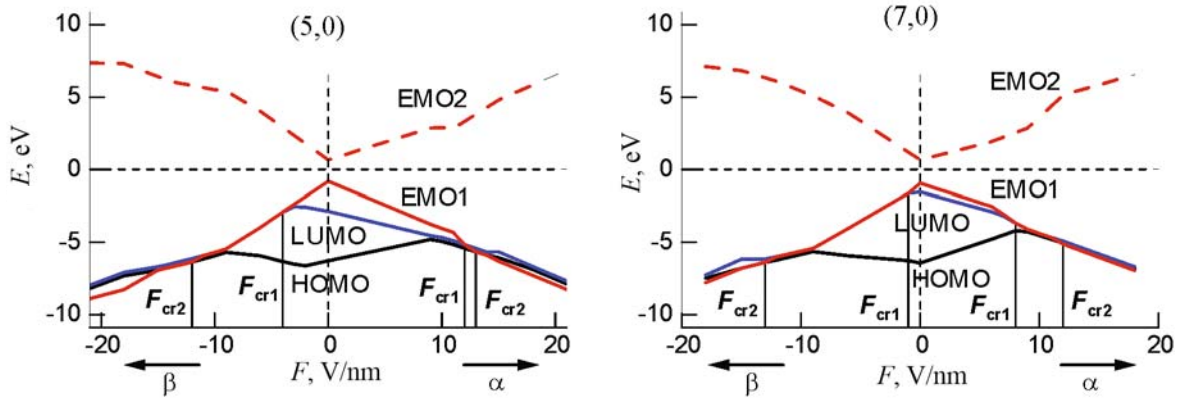

Fig. 5. Dependence of energy E of boundary and emission molecular orbitals of BN-nanotubes of the *zigzag* type (n,0) (i = 6) on electric field strength F and direction α, β.

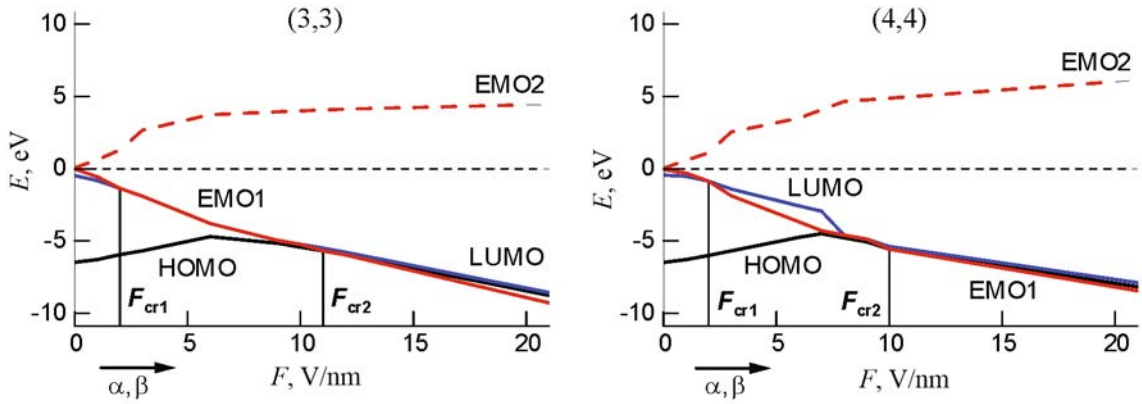

Fig. 6. Dependence of energy of boundary molecular orbitals and emission molecular orbitals of BN-nanotubes of the *armchair* type (n,n) (i = 6) on external electric field strength F.

and the direction of the applied electric field strength vector. However, the critical strength F_{cr1} decreased with increasing diameter of BNNTs of type (n,0). Also, strength F_{cr1} for type (n,0) BNNTs was affected by the direction of the electric field strength vector. For example, the EMO energy reached the LUMO energy at significantly weaker fields when the electric field strength vector was directed to the side of the B–H terminal fragment of a BNNT (β direction of the electric field strength vector). Note that type (n,n) BNNTs had a smaller F_{cr2} than type (n,0) nanotubes.

Table 5 shows that the critical strengths ensuring onset of field emission decreased asymptotically upon increasing the length of the nanotubes. Analogous results were obtained earlier for CNTs [47]. The effect of the electric field strength vector direction on the F_{cr1} and F_{cr2} values was observed in model BNNTs of chirality (n,0) with small linear length. Note that the critical field strength ensuring electron emission was smaller when vector F_{cr1} had the β direction than for the α direction.

An increase in the lengths of the conjugated system of rings in type (n,0) BNNTs consisting of many cyclic fragments nullified the difference between the F_{cr2} values for different directions of the electric field strength vector. However, the F_{cr1} values differed by ≈8 V/nm regardless of the diameter and length of type (n,0) BNNTs with different directions of $F_{\alpha\beta}$ (Fig. 3). This could be explained by the energy in the electric field decreasing more for an EMO localized on a terminal nanotube fragment containing a B–H bond than an N–H terminal fragment.

TABLE 4. Critical Strengths F_{cr1} and F_{cr2} (V/nm) of Constant Electric Field Ensuring Transition of Emission Orbitals into LUMO and HOMO for Model (i = 6) Carbon and Boron-Nitride Nanotubes

Nanotube type	Direction of electric field strength F	Chirality index							
		(5,0)		(7,0)		(3,3)		(4,4)	
		F_{cr1}	F_{cr2}	F_{cr1}	F_{cr2}	F_{cr1}	F_{cr2}	F_{cr1}	F_{cr2}
CNT [47]	α = β	9	13	10	19	5	11	6	11
BNNT	α	12	13	8	12	2	11	2	10
	β	4	12	1	13				

TABLE 5. Critical Strengths F_{cr1} and F_{cr2} (V/nm) of Constant Electric Field Ensuring Transition of Emission Orbitals into LUMO and HOMO for Model BN-Nanotubes of Various Lengths (Fig. 3)

Nanotube length	Direction of electric field strength F	Chirality index							
		(5,0)		(7,0)		(3,3)		(4,4)	
		F_{cr1}	F_{cr2}	F_{cr1}	F_{cr2}	F_{cr1}	F_{cr2}	F_{cr1}	F_{cr2}
i = 2	α	14	3	8	30	2	25	1	24
	β	6	25	1	29				
i = 4	α	12	17	8	17	2	14	2	14
	β	5	16	1	15				
i = 6	α	12	13	8	12	2	11	2	10
	β	4	12	1	13				

Conclusions. Numerical calculations by quantum chemistry methods showed the field electron emitters based on short single-walled BNNTs had several advantages over CNTs, i.e., 1) the strength of the constant electric field required for field emission from BNNTs was less than from CNTs of the same chirality, diameter, and length; 2) the emission properties of BNNTs were practically independent of their diameter.

Acknowledgment. The work was supported by the State Program of Scientific Research of the Republic of Belarus "Convergence-2025."

REFERENCES

1. Z. Ya. Kosakovskaya, S. V. von Gratowski, V. V. Koledov, V. G. Shavrov, A. M. Smolovich, A. P. Orlov, and J.-G. Liang, *J. Radio Electron.*, No. 12, 1–13 (2022); doi: 10.30898/1684-1719.2022.12.9.
2. N. Gupta, S. M. Gupta, and S. K. Sharma, *Carbon Lett.*, **29**, No. 5, 419–447 (2019); doi: 10.1007/s42823-019-00068-2.
3. A. A. Talin, K. A. Dean, and J. E. Jaskie, *Solid-State Electron.*, **45**, No. 6, 963–976 (2001); doi: 10.1016/S0038-1101(00)00279-3.
4. X. Cao, C. Lau, Y. Liu, F. Wu, H. Gui, Q. Liu, Y. Ma, H. Wan, M. R. Amer, and C. Zhou, *ACS Nano*, **10**, No. 11, 9816–9822 (2016); doi: 10.1021/acsnano.6b05368.
5. L. Camilli and M. Passacantando, *Chemosensors*, **6**, No. 4, 62 (1–17) (2018); doi: 10.3390/chemosensors6040062.
6. M. N. Norizan, M. H. Moklis, S. Z. N. Demon, N. A. Halim, A. Samsuri, I. S. Mohamad, V. F. Knight, and N. Abdullah, *RSC Adv.*, **10**, No. 71, 43704–43732 (2020); doi: 10.1039/D0RA09438B.
7. J. Chen, S. Z. Deng, and N. S. Xu, *Ultramicroscopy*, **95**, Nos. 1–4, 81–84 (2003); doi: 10.1016/S0304-3991(02)00300-5.
8. X. He, H. Htoon, S. K. Doorn, W. H. P. Pernice, F. Pyatkov, R. Krupke, A. Jeantet, Y. Chassagneux, and C. Voisin, *Nat. Mater.*, **17**, No. 8, 663–670 (2018); doi: 10.1038/s41563-018-0109-2.

9. R. H. Fowler and L. Nordheim, *Proc. R. Soc. London, Ser. A*, **119**, No. 781, 173–181 (1928); doi: 10.1098/rspa.1928.0091.
10. Z. Li, S. Deng, and N. Xu, *Front. Phys. China*, **1**, No. 3, 305–316 (2006); doi: 10.1007/s11467-006-0029-5.
11. D. S. Bychenok and G. Ya. Slepyan, *Vestn. BGU, Ser. 1*, No. 3, 33–36 (2012); http://elib.bsu.by/handle/123456789/49212.
12. P. G. Collins and A. Zettl, *Phys. Rev. B: Condens. Matter Mater. Phys.*, **55**, No. 15, 9391–9399 (1997); doi: 10.1103/PhysRevB.55.9391.
13. S. Dimitrijevic, J. C. Withers, V. P. Mammana, O. R. Monteiro, J. W. Ager, III, and I. G. Brown, *Appl. Phys. Lett.*, **75**, No. 17, 2680–2682 (1999); doi: 10.1063/1.125122.
14. X. Xu and G. R. Brandes, *Appl. Phys. Lett.*, **74**, No. 17, 2549–2551 (1999); doi: 10.1063/1.123894.
15. E. D. Eidelman and A. V. Arkhipov, *Phys. Usp.*, **63**, No. 7, 648–667 (2020); doi: 10.3367/UFNe.2019.06.038576.
16. R. Gao, Z. Pan, and Z. L. Wang, *Appl. Phys. Lett.*, **78**, No. 12, 1757–1759 (2001); doi: 10.1063/1.1356442.
17. J.-M. Bonard, T. Stockli, F. Maier, W.A. de Heer, A. Chatelain, J.-P. Salvetat, and L. Forro, *Phys. Rev. Lett.*, **81**, No. 7, 1441–1444 (1998); doi: 10.1103/PhysRevLett.81.1441.
18. X. H. Yang, H. I. Ma, and F. G. Zeng, *Vacuum*, **167**, 113–117 (2019); doi: 10.1016/j.vacuum.2019.06.001.
19. O. Groning, O. M. Kuttel, Ch. Emmenegger, P. Groning, and L. Schlapbach, *J. Vac. Sci. Technol. B*, **18**, No. 2, 665–678 (2000); doi: 10.1116/1.591258.
20. Yu. G. Polynskaya, A. S. Sinitsa, S. A. Vyrko, O. Ori, A. M. Popov, A. A. Knizhnik, N. A. Poklonski, and Yu. E. Lozovik, *Phys. E*, **148**, Article ID 115624 (1–7) (2023); doi: 10.1016/j.physe.2022.115624.
21. D. L. Carroll, P. Redlich, P. M. Ajayan, J. C. Charlier, X. Blase, A. De Vita, and R. Car, *Phys. Rev. Lett.*, **78**, No. 14, 2811–2814 (1997); doi: 10.1103/PhysRevLett.78.2811.
22. P. Kim, T. W. Odom, J.-L. Huang, and C. M. Lieber, *Phys. Rev. Lett.*, **82**, No. 6, 1225–1228 (1999); doi: 10.1103/PhysRevLett.82.1225.
23. K. A. Dean and B. R. Chalamala, *Appl. Phys. Lett.*, **76**, No. 3, 375–377 (2000); doi: 10.1063/1.125758.
24. R. C. Smith, D. C. Cox, and S. R. P. Silva, *Appl. Phys. Lett.*, **87**, No. 10, Article ID 103112 (1–3) (2005); doi: 10.1063/1.2041824.
25. S. Han and J. Ihm, *Phys. Rev. B: Condens. Matter Mater. Phys.*, **66**, No. 24, Article ID 241402 (1–4) (2002); doi: 10.1103/PhysRevB.66.241402.
26. J. Peng, Z. Li, C. He, S. Deng, N. Xu, X. Zheng, and G. Chen, *Phys. Rev. B: Condens. Matter Mater. Phys.*, **72**, No. 23, Article ID 235106 (1–8) (2005); doi: 10.1103/PhysRevB.72.235106.
27. O. B. Tomilin, E. V. Rodionova, and E. A. Rodin, *Russ. J. Phys. Chem. A*, **94**, No. 8, 1657–1662 (2020); doi: 10.1134/S0036024420080269.
28. O. B. Tomilin, E. V. Rodionova, E. A. Rodin, N. A. Poklonski, I. I. Anikeev, and S. V. Ratkevich, *Phys. Solid State*, **64**, No. 3, 359–364 (2022); doi: 10.21883/PSS.2022.03.53191.201.
29. O. B. Tomilin, I. V. Stankevich, E. E. Muryumin, and E. V. Rodionova, *Carbon*, **50**, No. 14, 5217–5225 (2012); doi: 10.1016/j.carbon.2012.07.005.
30. P. v. R. Schleyer, H. Jiao, M. N. Glukhovtsev, J. Chandrasekhar, and E. Kraka, *J. Am. Chem. Soc.*, **116**, No. 22, 10129–10134 (1994); doi: 10.1021/ja00101a035.
31. Al. A. Zakhidov, R. Nanjundaswamy, M. Zhang, S. B. Lee, A. N. Obraztsov, A. Cunningham, and A. A. Zakhidov, *J. Appl. Phys.*, **100**, No. 4, Article ID 044327 (2006); doi: 10.1063/1.2335780.
32. N. Danne, M. Kim, A. G. Godin, H. Kwon, Z. Gao, X. Wu, N. F. Hartmann, S. K. Doorn, B. Lounis, Y. Wang, and L. Cognet, *ACS Nano*, **12**, No. 6, 6059–6065 (2018); doi: 10.1021/acsnano.8b02307.
33. I. Muz and M. Kurban, *J. Alloys Compd.*, **802**, 25–35 (2019); doi: 10.1016/j.jallcom.2019.06.210.
34. J. H. Kim, T. V. Pham, J. H. Hwang, C. S. Kim, and M. J. Kim, *Nano Convergence*, **5**, 17 (1–13) (2018); doi: 10.1186/s40580-018-0149-y.
35. N. Kostoglou, C. Tampaxis, G. Charalambopoulou, G. Constantinides, V. Ryzhkov, C. Doumanidis, B. Matovic, C. Mitterer, and C. Rebholz, *Nanomaterials*, **10**, No. 12, 2435 (1–9) (2020); doi: 10.3390/nano10122435.
36. K. N. Yun, Y. Sun, J. S. Han, Y.-H. Song, and C. J. Lee, *ACS Appl. Mater. Interfaces*, **9**, No. 2, 1562–1568 (2017); https://doi.org/10.1021/acsami.6b10713.
37. M. W. Schmidt, K. K. Baldridge, J. A. Boatz, S. T. Elbert, M. S. Gordon, J. H. Jensen, S. Koseki, N. Matsunaga, K. A. Nguyen, S. Su, T. L. Windus, M. Dupuis, and J. A. Montgomery, Jr., *J. Comput. Chem.*, **14**, No. 11, 1347–1363 (1993); doi: 10.1002/jcc.540141112.
38. M. V. Kharlamova, *Phys. Usp.*, **56**, No. 11, 1047–1073 (2013); doi: 10.3367/UFNe.0183.201311a.1145.

39. Y.-M. Chou, H.-W. Wang, Y.-J. Lin, W.-H. Chen, and B.-C. Wang, *Diamond Relat. Mater.*, **18**, No. 2, 351–354 (2009); doi: 10.1016/j.diamond.2008.10.026.
40. A. S. Barnard, I. K. Snook, and S. P. Russo, *J. Mater. Chem.*, **17**, No. 28, 2892–2898 (2007); doi: 10.1039/b704037g.
41. G. Cassabois, P. Valvin, and B. Gil, *Nat. Photonics*, **10**, No. 4, 262–266 (2016); doi: 10.1038/nphoton.2015.277.
42. C. H. Lee, J. Wang, V. K. Kayatsha, J. Y. Huang, and Y. K. Yap, *Nanotechnology*, **19**, No. 45, Article ID 455605 (1–5) (2008); doi: 10.1088/0957-4484/19/45/455605.
43. P. Jaffrennou, J. Barjon, J.-S. Lauret, A. Maguer, D. Golberg, B. Attal-Tretout, F. Ducastelle, and A. Loiseau, *Phys. Status Solidi B*, **244**, No. 11, 4147–4151 (2007); doi: 10.1002/pssb.200776109.
44. M. Ishigami, J. D. Sau, S. Aloni, M. L. Cohen, and A. Zettl, *Phys. Rev. Lett.*, **94**, No. 5, Article ID 056804 (1–4) (2005); doi: 10.1103/PhysRevLett.94.056804.
45. F. Zheng, G. Zhou, S. Hao, and W. Duan, *J. Chem. Phys.*, **123**, No. 12, Article ID 124716 (1–5) (2005); doi: 10.1063/1.2035097.
46. N. A. Poklonski, S. V. Ratkevich, S. A. Vyrko, E. F. Kislyakov, O. N. Bubel′, A. M. Popov, Yu. E. Lozovik, N. N. Hieu, and N. A. Viet, *Chem. Phys. Lett.*, **545**, 71–77 (2012); doi: 10.1016/j.cplett.2012.07.023.
47. O. B. Tomilin, E. V. Rodionova, and E. A. Rodin, *Russ. J. Phys. Chem. A*, **95**, No. 9, 1883–1885 (2021); doi.org/10.1134/S0036024421090296.
48. A. Mananes, F. Duque, A. Ayuela, M. J. Lopez, and J. A. Alonso, *Phys. Rev. B: Condens. Matter Mater. Phys.*, **78**, No. 3, Article ID 035432 (1–10) (2008); doi: 10.1103/PhysRevB.78.035432.